Integrated Guidance and Control Design of Wide-Area Hypersonic Vehicle Based on Dynamic Inversion

Ying Wang, Guangwen Li(✉), Shaobo Zhai, Haizheng Zhang, Jingyi Wang, and Qiuling Jia

School of Automation, Northwestern Polytechnical University, Xian 710072, Shaanxi, China
liguangwen@nwpu.edu.cn

Abstract. The hypersonic vehicles (HV) represented by the combined powered aerospace vehicle have the characteristics of strong coupling, uncertain aerodynamic parameters, and many control constraints during the ascent phase. The guidance system of HV couple with its trajectory control system strongly and the trajectory optimization and guidance system design process are interactive and complicated. In this paper, a three-dimensional integrated guidance and control algorithm based on dynamic inversion is proposed. The attitude loop controller and guidance controller are designed to establish a mapping relationship between the longitudinal and lateral channel commands and the control surface commands, height and lateral position control of HV can be controlled accurately. The simulation results show that the integrated guidance and control method of HV for the wide-area flight can track reference commands precisely.

Keywords: Hypersonic vehicle · integrated guidance and control · dynamic inversion control

1 Introduction

Hypersonic vehicle (HV) has the characteristics of strong coupling, fast time-varying, and strong uncertainty, which has a significant impact on navigation guidance and control system. The guidance and control technology for HV has become a research hotspot [1–3]. During wide-range flight, the aircraft undergoes rapid state changes, and the uncertainty of the flight environment and aerodynamic models is significantly increased, while unknown disturbances become more apparent. Traditional control methods often separate guidance and control systems in design, which not only fails to optimize the overall control performance of the system to the greatest extent but also cannot meet the control performance requirements of HV under wide-range conditions [4, 5]. Therefore, the design of its guidance and control system needs to consider the coupling characteristics of the guidance and control loops and the interaction between the centroid motion and the motion around the centroid.

Integrated guidance and control (IGC) is a method to solve the above problems by integrating the guidance loop and control loop as a whole and directly generating control

Chinese Society of Aeronautics and Astronautics (Ed.): CASTC 2023, LNME, pp. 372–381, 2024.
https://doi.org/10.1007/978-981-99-8861-7_38

commands for the actuators based on the motion state information of the aircraft [6]. It fully utilizes the coupling relationship between the loops to directly design an integrated law, which more closely integrates the guidance and control loops and is beneficial to improve the overall performance [7].

Currently, there are various design methods for IGC, such as optimal control [8], sliding mode control [9], backstepping [10, 11], etc. However, there are still some problems in current research. Regarding the IGC design, many studies adopt a separate design approach for each channel, ignoring the coupling relationship of channel motion. This design requires repeated iterations and a large number of simulation tests, which leads to a large design workload and complex process [12]. As far as the existing IGC design scenarios are concerned, the current research is mostly based on missiles, and the flight phase is mostly in the dive phase. There are few studies on HV and its ascent control [13, 14].

A novel three-dimensional IGC algorithm based on dynamic inverse control is proposed in this paper, which solves the strong coupling and high nonlinearity of HV on guidance and control in the wide-range flight state of ascent. Firstly, a nonlinear dynamic inverse attitude loop is designed to meet the requirements of wide-range flight, and the high-precision control of angular rate and airflow angle is realized. Then, the guidance control law is designed by using the dynamic inversion control method, and the trajectory can be tracked accurately. Finally, the nominal trajectory under the designed multi-constraint conditions is used as the target command, the IGC design of the ascent phase is comprehensively simulated and verified, and the height and position can be controlled precisely.

2 Six-Degree-of-Freedom Model of HV

In this section, the six-degree-of-freedom model of the target vehicle is established according to the kinematics and dynamics equations. The motion equations of the six-degree-of-freedom rigid body model are as follows

$$\begin{cases} \dot{V} = \dfrac{P\cos\alpha\cos\beta - X - mg\sin\theta}{m} \\ \dot{\theta} = \dfrac{P(\sin\alpha\cos\gamma_V + \cos\alpha\sin\beta\sin\gamma_V) + Y\cos\gamma_V - Z\sin\gamma_V - mg\cos\theta}{mV} \\ \dot{\psi}_V = \dfrac{P(\sin\alpha\sin\gamma_V - \cos\alpha\sin\beta\cos\gamma_V) + Y\sin\gamma_V + Z\cos\gamma_V}{-mV\cos\theta} \end{cases} \tag{1}$$

$$\begin{cases} \dot{x} = V\cos\theta\cos\psi_V \\ \dot{y} = V\sin\theta \\ \dot{z} = -V\cos\theta\sin\psi_V \end{cases} \tag{2}$$

$$\begin{cases} \dot{\omega}_x = \dfrac{J_y(M_x - J_{xy}\omega_x\omega_z + (J_y - J_z)\omega_z\omega_y) + J_{xy}(M_y + J_{xy}\omega_y\omega_z - (J_x - J_z)\omega_z\omega_x)}{J_xJ_y - J_{xy}^2} \\ \dot{\omega}_y = \dfrac{J_x(M_y + J_{xy}\omega_y\omega_z - (J_x - J_z)\omega_z\omega_x) + J_{xy}(M_x - J_{xy}\omega_x\omega_z + (J_y - J_z)\omega_z\omega_y)}{J_xJ_y - J_{xy}^2} \\ \dot{\omega}_z = \dfrac{1}{J_z}(M_z + J_{xy}\omega_x^2 + (J_x - J_y)\omega_x\omega_y - J_{xy}\omega_y^2) \end{cases} \tag{3}$$

$$\begin{cases} \dot{\alpha} = \omega_z - (\omega_x \cos\alpha - \omega_y \sin\alpha)\tan\beta + \dfrac{1}{mV\cos\beta}(-Y - P\sin\alpha + mg\cos\theta\cos\gamma_v) \\ \dot{\beta} = \omega_x \sin\alpha + \omega_y \cos\alpha + \dfrac{1}{mV}(Z - P\cos\alpha\sin\beta + mg\cos\theta\sin\gamma_v) \\ \dot{\gamma}_v = \dfrac{\cos\alpha}{\cos\beta}\omega_x - \dfrac{\sin\alpha}{\cos\beta}\omega_y + \dfrac{Y + P\sin\alpha}{mV}(\tan\beta + \tan\gamma\sin\mu) \\ + \dfrac{Z}{mV}\tan\gamma\cos\mu\cos\beta \ - \dfrac{g}{V}\cos\gamma\cos\mu\tan\beta - \dfrac{P\cos\alpha}{mV}\tan\gamma\cos\mu\sin\beta \end{cases} \tag{4}$$

$$\begin{cases} m_{now} = m_0 - \int_0^{t_{now}} \dot{m}(t)dt \\ P = P_0(t_{bst}) + S_e(p_0 - p_h) \end{cases}. \tag{5}$$

The model consists of 12 state variables $X = [V, \theta, \psi_v, x, y, z, \omega_x\, \omega_y\, \omega_z\, , \alpha, \beta, \gamma_v]$ and 3 control inputs $u = [\delta_P, \delta_Y, \delta_R]$, Eq. is the dynamic equation of the center of mass motion, where V, θ, and ψ_v are the velocity, angle of track and angle of yaw. Equation (2) is the kinematics equation of the center of mass motion, x, y, z are the displacement of the aircraft in the ground coordinate system. Eq. is the dynamic equation of motion around the center of mass, $\omega_x\, \omega_y\, \omega_z$ are the angular velocities. Eq. is the differential equation of airflow angle, α, β, γ_v are attack angle, sideslip angle and bank angle. $\delta_P, \delta_Y, \delta_R$ are pitch, yaw, roll rudder angle. In addition, X is the total axial force, Y is the total lift force, and Z is the total lateral force. The mass of the assembly decreases due to the loss of fuel. The mass loss rate can be calculated by first-order interpolation to obtain the total mass of the current assembly, In Eq., m_0 is the mass of the HV at the initial full load, m_{now} is the current mass of the HV, $\dot{m}(t)$ is the loss of fuel mass at each time. Actual engine thrust P as in Eq., P_0 is the ground thrust of the combined engine, the thrust data changes with time and the thrust is uncontrollable. The static thrust varies with the static pressure of the gas at the nozzle section, where p_0 is the ground atmospheric static pressure, p_h is the static pressure at the height of the HV, and S_e is the nozzle section area.

The force generated by the rudder of HV includes the aerodynamic force F_R and the force generated by the gas rudder F_G, The torque includes the aerodynamic moment M_R and the moment M_G provided by the gas rudder. The specific expressions are listed as follows

$$\begin{cases} \mathrm{F}_i = F_{\mathrm{Ri}} + \mathrm{F}_{\mathrm{Gi}} = -C_k Q_s S - \mathrm{F}'_k \\ M_i = \mathrm{M}_{\mathrm{Ri}} + \mathrm{M}_{\mathrm{Gi}} = (C_j Q_s S) + M_{Gi} \end{cases} \quad i = x, y, z \ \ k = A, N, Z \ j = l, n, m \tag{6}$$

where, C_A, C_N, C_Z are the aerodynamic resultant force coefficients. C_l, C_n, C_m are the aerodynamic resultant moment coefficients. $Q_s = 0.5\rho V^2$ is dynamic pressure, ρ is the current atmospheric density. S is the reference area. L is the reference length. $F_A{}', F_N{}', F_Z{}'$ are the axial forces, normal force and lateral force of the gas rudder. M_{Gx}, M_{Gy}, M_{Gz} are the resultant moments of the gas rudder in the body shafting.

3 IGC Design Based on Dynamic Inversion

The controlled state variables of the loop around the center of mass are relatively intuitive, which are angle of attack, sideslip angle, velocity inclination angle, and three-channel angular rate. The guidance loop can be realized by controlling the ballistic angle, and the controlled state variables of the center of mass and the center of mass are fully coupled and integrated. Nonlinear dynamic inversion control can decouple between channels without a complex gain schedule. Because the change of the controlled object parameters cannot affect its linear decoupling control structure and gains, nonlinear dynamic inversion is suitable for the control of the aircraft in a wide domain.

Based on the dynamic inversion, the hierarchical design for various subsystems is proposed in this paper. Firstly, the control law is designed by using the dynamic characteristics between the control surface and the angular velocity. Secondly, the relationship between the airflow angle and the angular rate is established. In the third step, connect the airflow angle to the trajectory angle. The fourth step is to map the trajectory angle to the lateral position and altitude. Lastly, the height and lateral position commands to be tracked are connected with the control surface, so that the attitude control commands are obtained by using the relative motion relationship information between the aircraft and the target trajectory, and the aircraft can accurately track the height and lateral position. The following intuitive IGC design model can be obtained. The structure diagram is illustrated in Fig. 1.

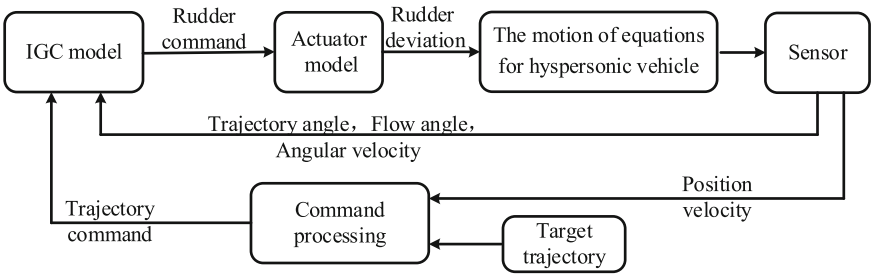

Fig. 1. IGC structural diagram.

3.1 Angular Rate Loop Design

The angular rate state of the aircraft is directly controlled by the control surface, so it is adopted as the inner loop of the control law. The differential equation can be written in the form of the following nonlinear system

$$\begin{cases} \dot{x}_1 = f_f(\bar{x}_f) + g_f(\bar{x}_f)u \\ y_1 = x_1 \end{cases} \tag{7}$$

where, $x_1 = [\omega_x, \omega_y, \omega_z]^T, \bar{x}_f = [V, \alpha, \beta, \omega_x, \omega_y, \omega_z]^T, u = [\delta_P, \delta_R, \delta_Y]^T$.

According to the differential Eq. (3) of angular rate, $f_f(\overline{x}_f))$ and $g_f(\overline{x}_f))$ can be obtained. As an example, the inversion expressions of the rolling rate ω_x are listed as follows

$$\begin{cases} f_{\omega_x}(\overline{x}_f) = \dfrac{J_y(\hat{M}_x - J_{xy}\omega_x\omega_z + (J_y - J_z)\omega_z\omega_y) + J_{xy}(\hat{M}_y + J_{xy}\omega_y\omega_z - (J_x - J_z)\omega_z\omega_x)}{J_xJ_y - J_{xy}^2} \\ g_{\omega_x i}(\overline{x}_f) = \dfrac{J_yC_{Mxi} + J_{xz}C_{Myi}}{J_xJ_y - J_{xy}^2}QSL, \quad i = \delta_P, \delta_R, \delta_Y \end{cases} \tag{8}$$

where,$\hat{M}_x$, $\hat{M}_y$ represent the rolling and yawing moment except the moment generated by the rudder deflection.

According to the characteristics of the aircraft and the actual engineering experience, this paper constructs the desired control signal: assuming that the error signal is: $\varepsilon = x_c\text{-}x$, x_c is a constant value, $\dot{x}_c$, $\ddot{x}_c$ are 0. What's more, $\ddot{\varepsilon} + 2\xi\omega_n\dot{\varepsilon} + \omega_n^2\varepsilon = 0$ is considered. When the error ε approaches 0, $\xi\omega_n > 0$ will be calculated. Then, ω_n^2, $2\xi\omega_n$ are replaced by k_i and k_p respectively, and the instruction model $x/x_c = k_i/(s^2 + k_ps + k_i)$ can be obtained. The desired rudder surface command is obtained by Eq. (9)

$$u = g_f^{-1}(\overline{x}_f)\left(\begin{bmatrix} k_{xi}\int(\omega_{xc} - \omega_x) - k_{\omega_x}\omega_x \\ k_{yi}\int(\omega_{yc} - \omega_y) - k_{\omega_y}\omega_y \\ k_{zi}\int(\omega_{zc} - \omega_z) - k_{\omega_z}\omega_z \end{bmatrix} - \begin{bmatrix} f_{\omega_x}(\overline{x}_f) \\ f_{\omega_y}(\overline{x}_f) \\ f_{\omega_z}(\overline{x}_f) \end{bmatrix}\right). \tag{9}$$

3.2 Airflow Angle Loop Design

In the design of the slower loop, the steering surface deflection effect is ignored, and the steady-state value of the fast loop is adopted instead of its instantaneous value. Therefore, the control law of the slower loop is an approximate inverse control law, which is written in a nonlinear form

$$\begin{cases} \dot{x}_2 = f_m(\overline{x}_m) + g_{m1}(\overline{x}_m)x_1 + g_{m2}(\overline{x}_m)u \\ y_2 = x_2 \end{cases} \tag{10}$$

where,$x_1 = [\omega_x, \omega_y, \omega_z]^T$,$\dot{x}_2 = [\dot{\alpha}, \dot{\beta}, \dot{\gamma}_V]^T$,$\overline{x}_m = [V, \gamma, \alpha, \beta, \gamma_V]^T$.

From the differential Eq. (4) of the airflow angle,$f_m(\overline{x}_m)$ and $g_m(\overline{x}_m)$ can be obtained. Based on the first-order filter, the angular rate expected command is established as

$$\begin{bmatrix} \omega_{xc} \\ \omega_{yc} \\ \omega_{zc} \end{bmatrix} = g_{m1}^{-1}(\overline{x}_m)\left(\begin{bmatrix} k_\alpha(\alpha_c - \alpha) + \dfrac{1}{\tau_\alpha s + 1}\dot{\alpha}_c \\ k_\beta(\beta_c - \beta) + \dfrac{1}{\tau_\beta s + 1}\dot{\beta}_c \\ k_{\gamma_v}(\gamma_{vc} - \gamma_v) + \dfrac{1}{\tau_{\gamma_v} s + 1}\dot{\gamma}_{vc} \end{bmatrix} - \begin{bmatrix} f_\alpha(\overline{x}_m) \\ f_\beta(\overline{x}_m) \\ f_{\gamma_v}(\overline{x}_m) \end{bmatrix}\right). \tag{11}$$

3.3 Trajectory Angle Loop Design

The Eq. (1) can be divided into Eq. (12) by balancing the horizontal and vertical forces. f_θ and $f_{\psi v}$ are minimal coupling quantities as Eq. (13)

$$\begin{cases} \dot{\theta} = \frac{Y\cos\gamma_V - mg}{mV} + f_\theta \\ \dot{\psi}_V = -\frac{Y\sin\gamma_V}{mV} + f_{\psi_V} \end{cases} \tag{12}$$

$$\begin{cases} f_\theta = \dfrac{mg(1-\cos\theta) + P(\sin\alpha\cos\gamma_V + \cos\alpha\sin\beta\sin\gamma_V) - Z\sin\gamma_V}{mV} \\ f_{\psi_V} = \dfrac{Y\sin\gamma_V}{mV} + \dfrac{P(\sin\alpha\sin\gamma_V - \cos\alpha\sin\beta\cos\gamma_V) + Y\sin\gamma_V + Z\cos\gamma_V}{-mV\cos\theta} \end{cases}. \tag{13}$$

The lift is expressed as

$$Y = QSC_{Y\alpha}\alpha + \Delta Y \tag{14}$$

where, $C_{Y\alpha}$ represents the derivative of the lift coefficient to the angle of attack, and ΔY represents the remaining lift.

Based on Eq. And Eq., the angle of attack command is simplified as Eq.

$$\alpha_c = ((-f_\theta + \dot{\theta}) + \frac{g}{V})\frac{mV}{\cos\gamma_V} - \Delta Y)\frac{1}{QSC_{Y\alpha}}. \tag{15}$$

The command value of the velocity inclination angle is obtained from Eq.

$$\gamma_V = arc\sin(\frac{mV(f_{\psi_V} - \dot{\psi}_V)}{Y}). \tag{16}$$

The designable control law based on Lyapunov stability theory is

$$\begin{cases} \dot{\theta} = \dot{\theta}_c - k_\theta(\theta - \theta_c) \\ \dot{\psi}_V = \dot{\psi}_c - k_{\psi_V}(\psi_V - \psi_{Vc}) \end{cases}. \tag{17}$$

In the ascent phase of HV, it should always maintain a non-sideslip state. Substituting Eq. Into Eq. and Eq., the desired command can be obtained. In summary, the expected command for establishing the aerodynamic angle can be obtained

$$\begin{cases} \alpha_c = ((-f_\theta + \dot{\theta}_c - k_\theta(\theta - \theta_c) + \frac{g}{V})\frac{mV}{\cos\gamma_V} - \Delta Y)\frac{1}{QSC_{Y\alpha}} \\ \beta_c = 0 \\ \gamma_{Vc} = arc\sin(\frac{mV(f_{\psi_V} - \dot{\psi}_{Vc} + k_{\psi_V}(\psi_V - \psi_{Vc}))}{Y}) \end{cases}. \tag{18}$$

3.4 Trajectory Loop Design

The purpose of the controller design in this section is to control the height and the lateral position, then the HV can track their respective expected commands. The uncoupled terms in the differential Eq. of the height and the lateral position are proposed separately, and the following equation can be obtained

$$\begin{cases} \dot{h} = V \sin\theta \\ \dot{z} = -V \sin\psi_V + f_z \end{cases}. \tag{19}$$

where, $f_z = V \sin\psi_V - V\cos\theta \sin\psi_V$.

Similarly, the control law is designed by using Lyapunov stability theory, and shift term of Eq. (19). The command value of the trajectory angle can be obtained

$$\begin{cases} \theta_c = \arcsin(\frac{\dot{h}_c - k_h(h-h_c)}{V}) \\ \psi_{Vc} = \arcsin(\frac{f_z - \dot{z}_c + k_z(z-z_c)}{V}) \end{cases}. \tag{20}$$

According to the motion state information of the aircraft, the control command required by the actuator is directly generated, that is, the relationship between the height and lateral position and the input control surface of the system is obtained, which integrates the guidance and control loop more closely and is conducive to improving the comprehensive performance.

4 Simulation Verification

In order to verify the designed guidance and control integrated controller can effectively deal with the HV in the ascent phase can better follow the designed trajectory command. In this paper, the Gauss pseudospectral method is applied to discretize the nonlinear differential equation and the nonlinear programming is adopted to solve the optimal open-loop reference trajectory. A trajectory command sequence meeting the constraint conditions is designed. By designing the optimal index, that is, the integration of normal and lateral overload in the whole ascent phase is minimized, the trajectory is smooth and the buffeting is minimized during the flight, which ensures the safety of the flight. The height and lateral position command sequences are obtained by interpolation of command values and time. The height varies from 10 km to 110 km, and the lateral position ranges from 0 to 3.1 km. The initial velocity is 3 Mach, and the initial trajectory inclination angle and pitch angle are 10°.

The initial values of aircraft parameters and controller parameters in the simulation are shown in Table 1 and 2, and the simulation results are shown in Fig. 2 , 3, 4, 5, 6 and 7.

Figure 3 is the response curve of the trajectory angle following the expected command. According to Fig. 3, the slight deviation in the front section of the response curve is mainly due to the influence of the velocity change and the reaction time of the controller. In general, the trajectory angle can follow the command curve accurately.

The dynamic response curve of the airflow angles and their command response curves are shown in Fig. 4, and the dynamic response curve of flight angular rate and

Table 1. Parameters of aircraft.

Parameter	Unit	Maximum weight	Empty weight
m	kg	23400	9060
S	m^2	1	1
L	m	11.575	11.575

Table 2. Parameters of controller.

Parameter	Value	Parameter	Value	Parameter	Value	Parameter	Value
k_{xi}	40	k_{ω_x}	13	k_β	0.9	τ_β	0
k_{yi}	40	k_{ω_y}	14	k_{γ_v}	1	τ_{γ_v}	0.1
k_{zi}	40	k_{ω_z}	20	k_θ	0.6	k_h	0.1
k_α	0.9	τ_α	0.5	k_{ψ_V}	0.35	k_z	0.04

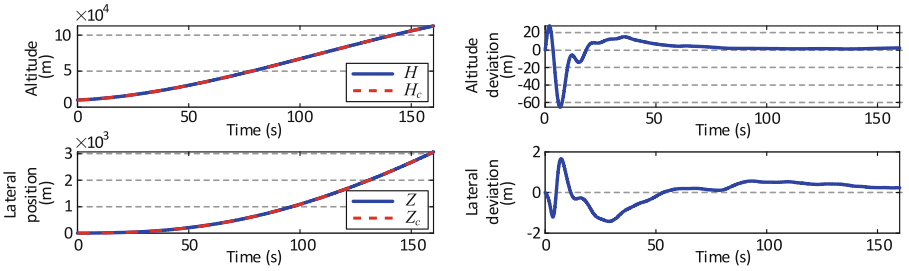

Fig. 2. Simulation results for trajectory response.

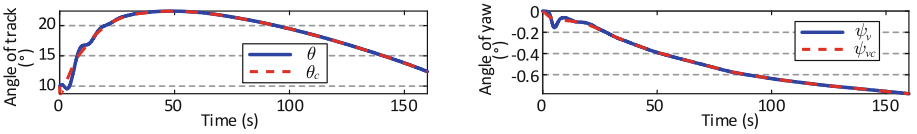

Fig. 3. Simulation results for trajectory angle.

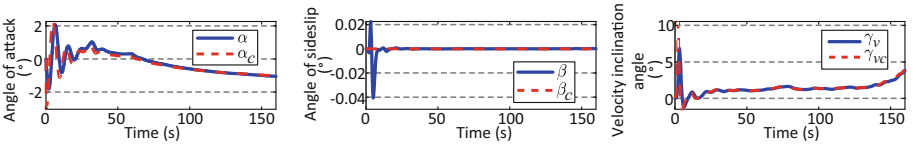

Fig. 4. Simulation results for airflow angle.

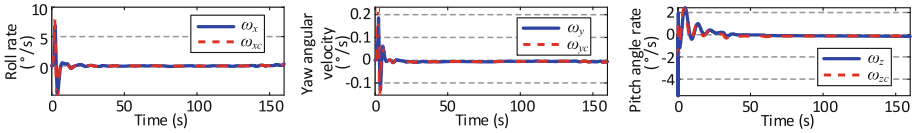

Fig. 5. Simulation results for angular velocity.

their command response curves are in Fig. 5. The sideslip angle remains at 0 almost throughout the ascent phase, and the fluctuation is so small that it can be ignored. The airflow angle and angular rate can better follow the command curve, because of response time, there will be a deviation from the command but does not affect the overall control effect.

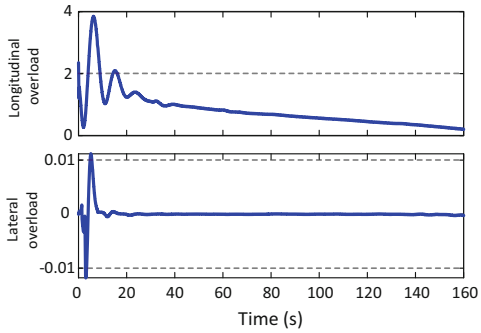

Fig. 6. Simulation results for overload.

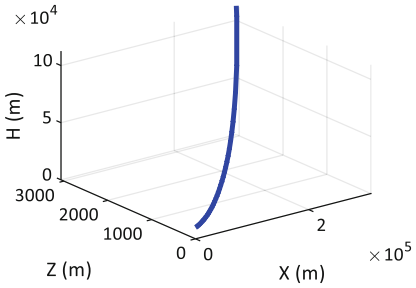

Fig. 7. Three-dimensional trajectory.

According to Fig. 6, the longitudinal overload variation range is within 4, and the lateral overload variation range is within 0.02, which remains stable and within the performance requirements. The flight three-dimensional trajectory, illustrated in Fig. 7, shows that the proposed algorithm ensures the stable control of the ascent phase of the HV.

5 Conclusion

In this paper, the IGC technology in the complicated and varied environment of the ascent phase is studied based on the wide-area flight of the HV. Firstly, a six-degree-of-freedom model of HV is established. Secondly, the IGC algorithm design of the ascent phase is completed by combining the block method of dynamic inversion. The height and lateral position commands to be tracked are connected with the control surface, and the relative motion relationship information between the aircraft and the target trajectory is adopted to obtain the control surface control commands, which directly realizes the tracking of the height and lateral moving position, and ensures the safety and stability of the aircraft. The simulation results show that the integrated controller proposed in this paper can realize the tracking of target height and lateral position in wide-area flight.

References

1. Gstattenbauer, G.J., Franke, M.E., Livingston, J.W.: Cost comparison of expendable hybrid and reusable launch vehicles. In: Proceedings of AIAA/Space Conferences and Exposition, San Jose (2006)
2. Wang, C.Q.: Technological innovation and development prospect of aerospace vehicle. J Astronaut, 2021, 42: 807–819Author, F., Author, S., Author, T.: Book title. 2nd edn. Publisher, Location (1999)
3. Bao, W.M.: Present situation and development tendency of aerospace control techniques. Acta Autom Sin **39**, 697–702 (2013)
4. Siouris, G.M.: Missile guidance and control systems. Springer Science & Business Media (2004)
5. Hou, M., Liang, X., Duan, G.: Adaptive block dynamic surface control for integrated missile guidance and autopilot. Chin. J. Aeronaut. **26**(3), 741–750 (2013)
6. Williams, D., Jack, R., Bernard, F.: Design of an integrated strapdown guidance and control system for a tactical missile. In: Guidance and Control Conference (1983)
7. Chwa, D., Jin Young, C.: Adaptive nonlinear guidance law considering control loop dynamics. IEEE Trans. Aerosp. Electron. Syst. **39**(4), 1134–1143 (2003)
8. Hughes, T., McFarland, M.: Integrated missile guidance law and autopilot design using linear optimal control. In: AIAA Guidance, Navigation, and Control Conference and Exhibit (2000)
9. Xu, H., Maj D.M., Ioannou, P.A.: Adaptive sliding mode control design for a hypersonic flight vehicle. J. Guidance, Contr., Dyn. **27**(5), 829–838 (2004)
10. Guo, C., Xiao-Geng, L.: Integrated guidance and control based on block backstepping sliding mode and dynamic control allocation. Proc. Inst. Mech. Eng., Part G: J. Aerosp. Eng. **229**(9) 1559–1574 (2015)
11. Zong, Q., et al.:Robust adaptive approximate backstepping control of a flexible air-breathing hypersonic vehicle with input constraint and uncertainty. Proceedings of the Institution of Mechanical Engineers, Part I: J. Syst. Contr. Eng. **228**(7), 521–539 (2014)
12. Wang, X., Wang, J.: Partial integrated guidance and control with impact angle constraints. J. Guidance, Contr. Dyn. **38**(5), 925–936 (2015)
13. Wang, J.H., Liu, L.H., Zhao, T., et al.: Integrated guidance and control for hypersonic vehicles in dive phase with multiple constraints. Aerosp. Sci. Technol. **53**, 103–115 (2016)
14. Song, H., Zhang, T.: Fast robust integrated guidance and control design of interceptors. IEEE Trans. Control Syst. Technol. **24**(1), 349–356 (2015)